ELSEVIER

Mechanics of Materials 30 (1998) 325–341

MECHANICS OF MATERIALS

A constitutive model for fcc crystals with application to polycrystalline OFHC copper

Sia Nemat-Nasser [a,*], Luqun Ni [a], Tomoo Okinaka [b]

[a] *Center of Excellence for Advanced Materials, Department of Applied Mechanics and Engineering Sciences, University of California, San Diego, 9500 Gilman Drive, La Jolla, CA 92093-0416, USA*

[b] *Department of Civil Engineering, Kinki University, 3-4-1 Kowakae Higashioosaka, Oosaka 577-8502, Japan*

Received 29 April 1997; received in revised form 7 July 1998

Abstract

Based on the results of a series of experiments on commercially pure OFHC copper (an fcc polycrystal), a physically based, rate- and temperature-dependent constitutive model is proposed for fcc single crystals. Using this constitutive model and the Taylor averaging method, numerical calculations are performed to simulate the experimental results for polycrystalline OFHC copper. The model calculation is based on a new efficient algorithm which has been successfully used to simulate the flow stress of polycrystalline tantalum over broad ranges of temperature, strain rate, and strain (Nemat-Nasser, S., Okinaka, T., Ni, L., 1998. J. Mech. Phys. Solids 46, 1009). The model effectively simulates a large body of experimental data, over a broad range of strain rates (0.001–8000 s^{-1}), and temperatures (77–1096 K), with strains close to 100%. Few adjustable constitutive parameters of the model are fixed at the outset for a given material. All other involved constitutive parameters are estimated based on the crystal structure and the physics of the plastic flow. © 1998 Published by Elsevier Science Ltd. All rights reserved.

1. Introduction

The kinematics of crystal plasticity has been developed by Hill (1966), Rice (1971), Hill and Rice (1972), and Hill and Havner (1982). Reviews and references are given by Havner (1992). Phenomenologically and empirically based constitutive relations of a power law and its variants are used by many authors to simulate the polycrystal response; see, e.g., Hutchinson (1976), Pan and Rice (1983), Peirce et al. (1983), Nemat-Nasser and Obata (1986), Rashid et al. (1992), Zikry and Nemat-Nasser (1990), and Anand and Kalidindi (1994).

Based on a series of experiments, Nemat-Nasser (1996) develops dislocation based constitutive models for the slip rates of fcc and bcc crystals. Continuum versions of the bcc and fcc model have been successfully applied to the commercially pure polycrystal tantalum and OFHC copper, by Nemat-Nasser and Isaacs (1997) and Nemat-Nasser and Li (1998), respectively. Recently, in Nemat-Nasser et al. (1998), using a new efficient algorithm proposed by Nemat-Nasser and Okinaka (1996), the dislocation-based model of Nemat-Nasser (1996) has been applied to represent rate- and temperature-dependent crystalline slip in bcc single-crystal

* Corresponding author. E-mail: sia@halebopp.ecsd.edu

0167-6636/98/$ – see front matter © 1998 Published by Elsevier Science Ltd. All rights reserved.
PII: S0167-6636(98)00055-6

tantalum, and the results are used to simulate the experimental data reported by Nemat-Nasser and Isaacs (1997) and Chen and Gray III (1996). Better correlation with the experimental results is achieved through the crystal plasticity model than the corresponding continuum counterpart.

In the present paper, a similar approach is used to model crystalline slip in fcc single crystals, and, using the Taylor averaging, to simulate the experimental data given by Nemat-Nasser and Li (1998) for OFHC copper. It turns out that the simulation using the crystal plasticity model provides a remarkably good correlation with the experimental results. Also, the results of the crystal plasticity model calculation is in good agreement with those of the continuum model calculation reported by Nemat-Nasser and Li (1998). The simulation based on the crystalline slip model produces excellent results for strain rates and temperatures from 0.001 to 8000 s^{-1} and 77 to 1096 K, respectively, with strains close to 100%. Most of the constitutive parameters are estimated on the basis of the crystal's microstructure, leaving only a few parameters to be evaluated empirically. These parameters are estimated at the outset, and then the resulting constitutive model is applied to all experimental data reported by Nemat-Nasser and Li (1998).

2. Fundamentals

2.1. Kinematics

In this section, we give a brief review of the kinematics of the finite deformation of crystals. The general account of elastic-plastic deformation of crystals at finite strains and rotations can be found in Hill (1966), Rice (1971), Hill and Rice (1972), Hill and Havner (1982), and, more recently, in Havner (1992).

The total deformation gradient, $\boldsymbol{F}$, measured with respect to the undeformed configuration of the crystal, is decomposed as

$$\boldsymbol{F} = \boldsymbol{F}^{*}\boldsymbol{F}^{\mathrm{p}}, \tag{2.1}$$

where the superscript $*$ and the superscript p represent the non-plastic (which is induced by elastic lattice distortion and rigid-body rotation) and the plastic (which is slip-induced) parts of the deformation, respectively; this notation is used throughout the paper.

The (total) velocity gradient is

$$\boldsymbol{L} \equiv \dot{\boldsymbol{F}}\boldsymbol{F}^{-1} = \boldsymbol{L}^{*} + \boldsymbol{F}^{*}\hat{\boldsymbol{L}}^{\mathrm{p}}\boldsymbol{F}^{*^{-1}}, \tag{2.2a}$$

where dot stands for the time derivative and the superscript -1 for the inverse, respectively; hat denotes that the velocity gradient is measured with respect to the *initial undeformed configuration* of the crystal lattice. In Eq. (2.2a), the non-plastic velocity gradient, $\boldsymbol{L}^{*}$, and the plastically-induced velocity gradient, $\hat{\boldsymbol{L}}^{\mathrm{p}}$, are respectively given by

$$\boldsymbol{L}^{*} = \dot{\boldsymbol{F}}^{*}\boldsymbol{F}^{*^{-1}} \tag{2.2b}$$

and

$$\hat{\boldsymbol{L}}^{\mathrm{p}} = \dot{\boldsymbol{F}}^{\mathrm{p}}\boldsymbol{F}^{\mathrm{p}^{-1}}. \tag{2.2c}$$

It is assumed, in this paper, that the plastic deformation is solely due to the crystalline slip. Then, the plastic velocity gradient, $\hat{\boldsymbol{L}}^{\mathrm{p}}$, is given as the sum of the slips on all slip systems. It is well-known that there are 12 primary slip systems in fcc single crystals. These are $\{1\,1\,1\}\,\langle 1\,1\,0\rangle$, $\{1\,1\,1\}\,\langle 1\,0\,1\rangle$, and $\{1\,1\,1\}\langle 0\,1\,1\rangle$. Hence,

$$\hat{\boldsymbol{L}}^{\mathrm{p}} = \sum_{\alpha=1}^{4}\sum_{a=1}^{3}\dot{\gamma}^{(\alpha a)}\boldsymbol{l}_{0}^{(\alpha a)}, \tag{2.3}$$

where the superscripts (αa) are the indices of the slip systems with $\alpha = 1, 2, 3, 4$ and $a = 1, 2, 3$ defining the slip planes and the slip directions on the corresponding slip plane, respectively. The numbering of the slip systems is listed in Table 1; $\dot{\gamma}^{(\alpha a)}$ is the (αa)th slip rate, and $\boldsymbol{l}_{0}^{(\alpha a)}$ defines the corresponding slip system, given by

$$\boldsymbol{l}_{0}^{(\alpha a)} = \boldsymbol{s}_{0}^{(\alpha a)} \otimes \boldsymbol{n}_{0}^{(\alpha)} \quad (\text{no sum on } \alpha). \tag{2.4}$$

In Eq. (2.4), $\boldsymbol{s}$ and $\boldsymbol{n}$ are unit vectors denoting the slip direction and the slip-plane normal, respectively, the subscript 0 stands for the initial configuration of the lattice.

For the present discussion, assume that the elastic strain is small, as is the case for most metals, including copper. By polar decomposition, we obtain

$$\boldsymbol{F}^{*} = \boldsymbol{V}^{*}\boldsymbol{R}^{*} \tag{2.5a}$$

Table 1
Numbering of slip systems

(11)	$(1\ 1\ 1)[\bar{1}\ 1\ 0]$	(31)	$(\bar{1}\ \bar{1}\ 1)[1\ \bar{1}\ 0]$
(12)	$(1\ 1\ 1)[0\ \bar{1}\ 1]$	(32)	$(\bar{1}\ \bar{1}\ 1)[0\ 1\ 1]$
(13)	$(1\ 1\ 1)[1\ 0\ \bar{1}]$	(33)	$(\bar{1}\ \bar{1}\ 1)[\bar{1}\ 0\ \bar{1}]$
(21)	$(\bar{1}\ 1\ 1)[\bar{1}\ \bar{1}\ 0]$	(41)	$(1\ \bar{1}\ 1)[1\ 1\ 0]$
(22)	$(\bar{1}\ 1\ 1)[1\ 0\ 1]$	(42)	$(1\ \bar{1}\ 1)[\bar{1}\ 0\ 1]$
(23)	$(\bar{1}\ 1\ 1)[0\ 1\ \bar{1}]$	(43)	$(1\ \bar{1}\ 1)[0\ \bar{1}\ \bar{1}]$

and then set

$$\boldsymbol{V}^* = \mathbf{1} + \boldsymbol{\varepsilon}, \tag{2.5b}$$

where the elastic strain, $\boldsymbol{\varepsilon}$, measured in the rotated lattice, is infinitesimally small; $\boldsymbol{R}^*$ is the rigid-body lattice rotation. With the assumption of small elastic strain, it follows that

$$\boldsymbol{L} = \boldsymbol{L}^* + \sum_{\alpha=1}^{4}\sum_{a=1}^{3}\dot{\gamma}^{(\alpha a)}\boldsymbol{l}^{(\alpha a)}, \tag{2.6a}$$

where

$$\boldsymbol{l}^{(\alpha a)} = \boldsymbol{R}^*\boldsymbol{l}_0^{(\alpha a)}\boldsymbol{R}^{*\mathrm{T}}. \tag{2.6b}$$

From Eq. (2.2b), Eqs. (2.5a) and (2.5b), the non-plastic velocity gradient is written as

$$\boldsymbol{L}^* = \dot{\boldsymbol{\varepsilon}} + \boldsymbol{\varepsilon}\boldsymbol{\Omega} - \boldsymbol{\Omega}^*\boldsymbol{\varepsilon} + \boldsymbol{\Omega}^*, \tag{2.7a}$$

where $\boldsymbol{\Omega}^*$ is the rigid-body lattice spin rate, defined by

$$\boldsymbol{\Omega}^* = \dot{\boldsymbol{R}}^*\boldsymbol{R}^{*\mathrm{T}}. \tag{2.7b}$$

The symmetric and antisymmetric parts of the total velocity gradient $\boldsymbol{L}$, are denoted by $\boldsymbol{D}$ and $\boldsymbol{W}$, respectively. Similarly, define the symmetric and antisymmetric parts of the rotated slip system tensor $\boldsymbol{l}^{(\alpha a)}$, by $\boldsymbol{p}^{(\alpha a)}$ and $\boldsymbol{w}^{(\alpha a)}$ respectively. Then

$$\boldsymbol{D} = \boldsymbol{D}^* + \sum_{\alpha=1}^{4}\sum_{a=1}^{3}\dot{\gamma}^{(\alpha a)}\boldsymbol{p}^{(\alpha a)} \tag{2.8a}$$

and

$$\boldsymbol{W} = \boldsymbol{W}^* + \sum_{\alpha=1}^{4}\sum_{a=1}^{3}\dot{\gamma}^{(\alpha a)}\boldsymbol{w}^{(\alpha a)}, \tag{2.8b}$$

where $\boldsymbol{D}^* = \dot{\boldsymbol{\varepsilon}} + \boldsymbol{\varepsilon}\boldsymbol{\Omega} - \boldsymbol{\Omega}^*\boldsymbol{\varepsilon}$ and $\boldsymbol{W}^* = \boldsymbol{\Omega}^*$ are the corresponding non-plastic deformation rate and spin, respectively.

2.2. Interdependency of slip systems

From the definitions Eqs. (2.4) and (2.6b) of the slip system tensor, $\boldsymbol{l}^{(\alpha a)}$ and $\boldsymbol{p}^{(\alpha a)}$ are traceless, since $\boldsymbol{s}^{(\alpha a)}$ and $\boldsymbol{n}^{(\alpha)}$ are orthogonal pairs. A three-dimensional symmetric second-order tensor with a zero trace, has only five independent components. Therefore, among the 12 $\boldsymbol{p}^{(\alpha a)}$'s in an fcc single crystal, there exist at least seven linear interdependency conditions.

The 12 slip systems may be divided into four families, according to the slip-plane normal directions $(1\ 1\ 1)$, $(\bar{1}\ 1\ 1)$, $(\bar{1}\ \bar{1}\ 1)$, and $(1\ \bar{1}\ 1)$. In each family, there are three slip systems, with one interdependency relation between them. For example, in the first family of slip systems (11), (12), and (13), the three slip directions $[\bar{1}\ 1\ 0]$, $[0\ \bar{1}\ 1]$, and $[1\ 0\ \bar{1}]$ form a closed contour, leading to the interdependency condition

$$\boldsymbol{p}^{(11)} + \boldsymbol{p}^{(12)} + \boldsymbol{p}^{(13)} = \mathbf{0}. \tag{2.9a}$$

For the remaining three families, there are three similar interdependency relations,

$$\boldsymbol{p}^{(21)} + \boldsymbol{p}^{(22)} + \boldsymbol{p}^{(23)} = \mathbf{0}, \tag{2.9b}$$

$$\boldsymbol{p}^{(31)} + \boldsymbol{p}^{(32)} + \boldsymbol{p}^{(33)} = \mathbf{0} \tag{2.9c}$$

and

$$\boldsymbol{p}^{(41)} + \boldsymbol{p}^{(42)} + \boldsymbol{p}^{(43)} = \mathbf{0}. \tag{2.9d}$$

Apart from the four interdependency conditions listed above, there are three more interdependency conditions between the $\boldsymbol{p}^{(\alpha a)}$'s. Using the method presented in Nemat-Nasser et al. (1998), the three additional conditions are found to be (see Appendix A)

$$-\boldsymbol{p}^{(11)} + \boldsymbol{p}^{(22)} + \boldsymbol{p}^{(43)} = \mathbf{0}, \tag{2.10a}$$

$$-\boldsymbol{p}^{(12)}-\boldsymbol{p}^{(33)}+\boldsymbol{p}^{(41)}=\boldsymbol{0}, \tag{2.10b}$$

$$\boldsymbol{p}^{(13)}-\boldsymbol{p}^{(21)}+\boldsymbol{p}^{(32)}=\boldsymbol{0}. \tag{2.10c}$$

3. Physically based model of crystalline slip

Slip occurs by the motion of dislocations on the corresponding slip plane and in the corresponding slip direction. In this process, dislocations have to overcome both short-range and long-range obstacles (Kocks et al., 1975). The short-range barriers may include the Peierls stress (the primary short-range resistance for bcc metals), point defects (vacancies and self-interstitials), other dislocations which intersect the slip plane (the primary short-range resistance for fcc metals), or substitutional atoms. The long-range barriers may include the elastic stress field due to grain boundaries, far-field forests of dislocations, and far-field defects. The resistance due to the short-range barriers may be overcome by thermal activation, while that due to the long-range barriers is, in essence, independent of temperature, and can be overcome with the aid of the applied resolved shear stress.

The flow stress, $\tau^{(\alpha a)}$, may therefore, be written as

$$\tau^{(\alpha a)}=\tau^{*(\alpha a)}+\tau_{\mathrm{a}}^{(\alpha a)}, \tag{3.1}$$

where $\tau^{*(\alpha a)}$ and $\tau_{\mathrm{a}}^{(\alpha a)}$, both associated with the (αa)th slip system, are the thermal and athermal parts corresponding to the short-range and long-range barriers to the motion of dislocations, respectively. The thermal part of the flow stress, $\tau^{*(\alpha a)}$, is a decreasing function of temperature of the single crystal, T, and an increasing function of the plastic strain rate, $\dot{\gamma}^{(\alpha a)}$. The athermal part of the flow stress, $\tau_{\mathrm{a}}^{(\alpha a)}$, is essentially independent of temperature, T, and the plastic strain rate, $\dot{\gamma}^{(\alpha a)}$, but it is affected by them in certain indirect ways (Nemat-Nasser and Li, 1998).

3.1. The thermal part of the flow stress

For a dislocation moving on the αth slip plane in the ath direction, the frequency of the occurrence of a jump over a short-range barrier is given by

$$\omega^{(\alpha a)}=\omega_0^{(\alpha a)}\exp\left(-\frac{\Delta G^{(\alpha a)}}{kT}\right), \tag{3.2}$$

where $\omega_0^{(\alpha a)}$, k, and T are the attempt frequency, Boltzman constant, and temperature, respectively, and $\Delta G^{(\alpha a)}$ is the activation energy, associated with the (αa)th slip system.

The total average time, t, that the dislocation travels between two neighboring sets of barriers, consists of two parts,

$$t=t_{\mathrm{w}}+t_{\mathrm{r}}, \tag{3.3}$$

where t_{w} is the waiting period before a dislocation crosses a barrier, and t_{r} is the running period that the dislocation moves until meeting the next barrier. Noting that the average travel distance is the sum of the average distance between barriers, d, and the average effective barrier width, λ, the average velocity of the motion of the dislocations is estimated by

$$\bar{v}\approx\frac{d+\lambda}{t_{\mathrm{w}}+t_{\mathrm{r}}}\approx\frac{d}{t_{\mathrm{w}}}, \tag{3.4a}$$

when $d\gg\lambda$ which is true when intersecting dislocations are the barriers, and $t_{\mathrm{w}}\gg t_{\mathrm{r}}$ which is the case in general. For the (αa)th slip system, the waiting period, t_{w}, is approximately given by

$$t_{\mathrm{w}}^{(\alpha a)}\approx 1/\omega^{(\alpha a)}. \tag{3.4b}$$

Hence, using the frequency given by Eq. (3.2), from Eq. (3.4b) the average dislocation velocity for the (αa)th slip system may be approximated by

$$\bar{v}^{(\alpha a)}\approx d^{(\alpha a)}\omega^{(\alpha a)}=d^{(\alpha a)}\,\omega_0^{(\alpha a)}\exp\left(-\frac{\Delta G^{(\alpha a)}}{kT}\right). \tag{3.5}$$

The slip rate, $\dot{\gamma}^{(\alpha a)}$, of the (αa)th slip system can therefore be expressed as

$$\dot{\gamma}^{(\alpha a)}=b^{(\alpha a)}\rho_{\mathrm{m}}^{(\alpha a)}\bar{v}^{(\alpha a)}, \tag{3.6a}$$

where $b^{(\alpha a)}$ is the magnitude of the corresponding Burgers vector and $\rho_{\mathrm{m}}^{(\alpha a)}$ is the density of the mobile dislocations associated with the (αa)th slip system. Combining the last equation with Eq. (3.5), the slip rate, $\dot{\gamma}^{(\alpha a)}$, is given by

$$\dot{\gamma}^{(\alpha a)}=\dot{\gamma}_{\mathrm{r}}^{(\alpha a)}\exp\left(-\frac{\Delta G^{(\alpha a)}}{kT}\right), \tag{3.6b}$$

where

$$\dot{\gamma}_{\mathrm{r}}^{(\alpha a)} \equiv b^{(\alpha a)} d^{(\alpha a)} \rho_{\mathrm{m}}^{(\alpha a)} \omega_0^{(\alpha a)} \tag{3.6c}$$

is the reference slip rate.

Following Kocks et al. (1975), in terms of the thermal part of the flow stress, the activation energy, $\Delta G^{(\alpha a)}$, is represented by

$$\Delta G^{(\alpha a)} = G_0^{(\alpha a)} \left\{ 1 - \left(\frac{\tau^{*(\alpha a)}}{\hat{\tau}^{(\alpha a)}} \right)^p \right\}^q, \tag{3.7a}$$

where

$$\hat{\tau}^{(\alpha a)} = \tau^{*(\alpha a)}|_{T=0} \tag{3.7b}$$

is the threshold shear stress which is the stress required by a dislocation to overcome the barrier without any assistance from the thermal activation;

$$G_0^{(\alpha a)} = \hat{\tau}^{(\alpha a)} V^* \equiv \hat{\tau}^{(\alpha a)} b^{(\alpha a)} \lambda^{(\alpha a)} d^{(\alpha a)}, \tag{3.7c}$$

is the total free energy needed to overcome the barrier without the aid of external work; and $V^* \equiv b^{(\alpha a)} \lambda^{(\alpha a)} d^{(\alpha a)}$ is the activation volume. The constants p and q in Eq. (3.7a) are the parameters defining the shape of the energy-barrier profile.

From Eqs. (3.6b) and (3.7a), it follows that

$$\tau^{*(\alpha a)} = \hat{\tau}^{(\alpha a)} \left[1 - \left(- \frac{kT}{G_0^{(\alpha a)}} \ln \frac{\left|\dot{\gamma}^{(\alpha a)}\right|}{\dot{\gamma}_{\mathrm{r}}^{(\alpha a)}} \right)^{1/q} \right]^{1/p} \tag{3.8a}$$

for $T \leqslant T_{\mathrm{c}}^{(\alpha a)}$, and

$$\tau^{*(\alpha a)} = 0, \quad \text{for } T > T_{\mathrm{c}}^{(\alpha a)}, \tag{3.8b}$$

where

$$T_{\mathrm{c}}^{(\alpha a)} = -G_0^{(\alpha a)} / \{ k \ln [|\dot{\gamma}^{(\alpha a)}| / \dot{\gamma}_{\mathrm{r}}^{(\alpha a)}] \} \tag{3.8c}$$

is the critical temperature at which the dislocation can overcome its short-range barriers without the assistance of the applied resolved shear stress.

Examine Eq. (3.7c), where $G_0^{(\alpha a)}$ and $b^{(\alpha a)}$ are constants, and λ is dependent on the profile of the barrier. The average distance between barriers, $d^{(\alpha a)}$, depends on the type of the barrier. For Peierls barriers, which are the primary short-range obstacles of bcc metals, $d^{(\alpha a)} = b^{(\alpha a)}$. For fcc crystals, the short-range barriers to the motion of dislocations primarily are the dislocation forests which intersect the slip plane. In this case, the average distance between barriers, $d^{(\alpha a)}$, is the same as the average spacing, $l^{(\alpha a)}$, of the dislocations which intersect the slip plane. Hence, $d^{(\alpha a)} = l^{(\alpha a)}$ is a function of the current density of dislocations, $\rho_{\mathrm{c}}^{(\alpha a)}$, associated with the (αa)th slip system, and one has

$$d^{(\alpha a)} = l^{(\alpha a)} \approx [\rho_{\mathrm{c}}^{(\alpha a)}]^{-1/2}. \tag{3.9}$$

The current density of dislocations, $\rho_{\mathrm{c}}^{(\alpha a)}$, associated with the (αa)th slip system, is defined by the accumulated dislocations which intersect the αth slip plane. Hence, it depends on both the plastic strain, $\gamma_{\mathrm{I}}^{(\alpha a)}$, produced by the slips on the "intersecting" slip planes [1] and the temperature: the greater $\gamma_{\mathrm{I}}^{(\alpha a)}$, the larger $\rho_{\mathrm{c}}^{(\alpha a)}$; the higher temperature, the smaller $\rho_{\mathrm{c}}^{(\alpha a)}$. The following approximation is therefore inferred from Nemat-Nasser/Li continuum model:

$$d^{(\alpha a)} = l^{(\alpha a)} = l_0^{(\alpha a)} / f(\gamma_{\mathrm{I}}^{(\alpha a)}, T), \tag{3.10a}$$

$$f(\gamma_{\mathrm{I}}^{(\alpha a)}, T) > 0, \quad f(0, T_0) = 1, \tag{3.10b}$$

$$\frac{\partial f(\gamma_{\mathrm{I}}^{(\alpha a)}, T)}{\partial \gamma_{\mathrm{I}}^{(\alpha a)}} \geqslant 0, \quad \frac{\partial f(\gamma_{\mathrm{I}}^{(\alpha a)}, T)}{\partial T} \leqslant 0, \tag{3.10c}$$

where $l_0^{(\alpha a)}$ is the initial average spacing of the dislocations intersecting the slip plane, T_0 is the initial temperature, and the plastic strain, $\gamma_{\mathrm{I}}^{(\alpha a)}$, produced by the slips on the intersecting slip planes is given by

$$\gamma_{\mathrm{I}}^{(\alpha a)} = \sum_{\beta:\mathrm{ISP}} \sum_{b=1}^{3} K_{(\beta b)}^{(\alpha a)} \int_0^t \left| \dot{\gamma}^{(\beta b)}(\xi) \right| \mathrm{d}\xi. \tag{3.10d}$$

Here the first summation is performed over all intersecting slip planes (ISP). The coefficients $K_{(\beta b)}^{(\alpha a)}$ in this equation may be calculated from the density and distribution of the dislocations on the intersecting slip planes, following Stroh (1953) and Zarka (1968). Again, based on the continuum model, consider the simple model

$$f = 1 + a^{(\alpha a)}(T) [\gamma_{\mathrm{I}}^{(\alpha a)}]^{n_0} \tag{3.11a}$$

with

[1] An intersecting slip plane is a plane whose dislocations pierce the considered slip plane.

$$a^{(\alpha a)}(T) = a_0^{(\alpha a)}[1 - (T/T_m)^2], \tag{3.11b}$$

where T_m is the melting temperature ($\approx$1350 K for copper). In Eqs. (3.11a) and (3.11b), $a_0^{(\alpha a)}$ is a non-negative constant depending on the initial dislocation (barrier) spacing, and n_0 is a constant between 0 and 1. These constants are considered to be adjustable constitutive parameters.

Now from the relation Eq. (3.7c), noting that $G_0^{(\alpha a)}$ is constant, it follows that

$$\hat{\tau}^{(\alpha a)} = \hat{\tau}_0^{(\alpha a)} f(\gamma_I^{(\alpha a)}, T) \tag{3.12a}$$

with

$$\hat{\tau}_0^{(\alpha a)} = G_0^{(\alpha a)}/[b^{(\alpha a)}\lambda^{(\alpha a)} l_0^{(\alpha a)}]. \tag{3.12b}$$

The threshold shear stress now takes on the value $\hat{\tau}_0^{(\alpha a)} f(\gamma_I^{(\alpha a)}, 0)$.

To obtain the plastic strain rate, use Eq. (3.10a) in Eq. (3.6c), leading to

$$\dot{\gamma}_r^{(\alpha a)} = \dot{\gamma}_0^{(\alpha a)}/f(\gamma_I^{(\alpha a)}, T), \tag{3.13a}$$

with

$$\dot{\gamma}_0^{(\alpha a)} \equiv b^{(\alpha a)}\rho_m^{(\alpha a)}\omega_0^{(\alpha a)} l_0^{(\alpha a)}. \tag{3.13b}$$

Consequently, when the dislocation forests intersecting the slip plane are the primary short-range obstacles, as for fcc crystals, the thermal part of the flow stress is obtained as

$$\tau^{*(\alpha a)} = \hat{\tau}_0^{(\alpha a)} f(\gamma_I^{(\alpha a)}, T)\left\{1 - \left[-\frac{kT}{G_0^{(\alpha a)}} \times \left(\ln \frac{\left|\dot{\gamma}^{(\alpha a)}\right|}{\dot{\gamma}_0^{(\alpha a)}} + \ln f(\gamma_I^{(\alpha a)}, T) \right) \right]^{1/q} \right\}^{1/p},$$

$$\text{for } T \leqslant T_c^{(\alpha a)}, \tag{3.14a}$$

and

$$\tau^{*(\alpha a)} = 0 \quad \text{for } T > T_c^{(\alpha a)}, \tag{3.14b}$$

where the critical temperature $T_c^{(\alpha a)}$ is determined by the following equation

$$T_c^{(\alpha a)} = -G_0^{(\alpha a)}/\{k \ln[|\dot{\gamma}^{(\alpha a)}|f(\gamma_I^{(\alpha a)}, T_c^{(\alpha a)})/\dot{\gamma}_0^{(\alpha a)}]\}. \tag{3.14c}$$

3.2. The athermal part of the flow stress

As explained before, the athermal part of the flow stress, $\tau_a^{(\alpha a)}$, represents the resistance to the mobile dislocation generated by the elastic stress field of the long-range barriers, such as other dislocations. A dislocation can overcome such obstacles with the aid of the applied resolved shear stress. Assume that $\tau_a^{(\alpha a)}$ is a function of the plastic strain, $\gamma^{(\alpha a)}$, the average grain size, $d_G^{(\alpha a)}$, and possibly other parameters, and write

$$\tau_a^{(\alpha a)} = g^{(\alpha a)}(\gamma^{(\alpha a)}, d_G^{(\alpha a)}, \ldots)\tau_{a1}^{(\alpha a)}. \tag{3.15}$$

As an example, consider a simple model,

$$\tau_a^{(\alpha a)} = \tau_{a0}^{(\alpha a)} + [(\gamma^{(\alpha a)})^{n_1} + k_0 (d_G^{(\alpha a)})^{-1/2}]\tau_{a1}^{(\alpha a)}, \tag{3.16}$$

where $\tau_{a0}^{(\alpha a)}$, $\tau_{a1}^{(\alpha a)}$, n_1, and k_0 are constants, and $\gamma^{(\alpha a)}$ the calculated plastic strain associated with the (αa)th slip system, defined by

$$\gamma^{(\alpha a)} = \sum_{\beta=1}^{4}\sum_{b=1}^{3} K_{(\beta b)}^{(\alpha a)} \int_0^t \left|\dot{\gamma}^{(\beta b)}(\xi)\right| \, d\xi. \tag{3.17}$$

Again, the coefficients $K_{(\beta b)}^{(\alpha a)}$ may be computed from the density and distribution of the dislocations, following Stroh (1953) and Zarka (1968). Note that, in Eqs. (3.16) and (3.17) $\gamma^{(\alpha a)}$ corresponds to all accumulated plastic slips, whereas in the thermally activated case, only the intersecting dislocations and hence $\gamma_I^{(\alpha a)}$ contribute to the barriers' spacing; see Eqs. (3.10a) and (3.10d).

3.3. The constitutive relation

From Eqs. (3.14a), (3.14b), (3.15) and since the slip rate, $\dot{\gamma}^{(\alpha a)}$, and the driving shear stress, $\tau^{(\alpha a)}$, have the same sign, the resistance to slip of the (αa)th slip system is given by

$$\tau^{(\alpha a)} = \operatorname{sgn}(\dot{\gamma}^{(\alpha a)})\{g^{(\alpha a)}(\gamma^{(\alpha a)}, d_G^{(\alpha a)}, \ldots)\tau_{a1}^{(\alpha a)} + \hat{\tau}_0^{(\alpha a)} f(\gamma_I^{(\alpha a)}, T) \times \left[1 - \left(-\frac{kT}{G_0^{(\alpha a)}} \ln \frac{\left|\dot{\gamma}^{(\alpha a)}\right| f(\gamma_I^{(\alpha a)}, T)}{\dot{\gamma}_0^{(\alpha a)}} \right)^{1/q}\right]^{1/p}$$

$$\text{for } T \leqslant T_c^{(\alpha a)} \tag{3.18a}$$

and

$$\tau^{(\alpha a)} = \operatorname{sgn}(\dot\gamma^{(\alpha a)}) g^{(\alpha a)}(\gamma^{(\alpha a)}, d_{\mathrm{G}}^{(\alpha a)}, \ldots)\tau_{\mathrm{a1}}^{(\alpha a)} \quad \text{for } T > T_{\mathrm{c}}^{(\alpha a)}, \tag{3.18b}$$

where $T_{\mathrm{c}}^{(\alpha a)}$ is determined by Eq. (3.14c).

Consider now the example $f = 1 + a^{(\alpha a)}(T)\gamma_{\mathrm{I}}^{n_0}$ defined in Eq. (3.11a) for the dislocation spacing, so that $\hat\tau^{(\alpha a)}$ associated with the (αa)th slip system becomes

$$\hat\tau^{(\alpha a)} = \hat\tau_0^{(\alpha a)}[1 + a^{(\alpha a)}(T)\gamma_{\mathrm{I}}^{n_0}]. \tag{3.19}$$

Also simplify the athermal part of the flow stress to

$$\tau_{\mathrm{a}}^{(\alpha a)} = g^{(\alpha a)}(\gamma^{(\alpha a)}, d_{\mathrm{G}}^{(\alpha a)}, \ldots)\tau_{\mathrm{a1}}^{(\alpha a)} = \tau_{\mathrm{a0}}^{(\alpha a)} + \tau_{\mathrm{a1}}^{(\alpha a)}[\gamma^{(\alpha a)}]^{n_1}, \tag{3.20}$$

where $\tau_{\mathrm{a0}}^{(\alpha a)}$, $\tau_{\mathrm{a1}}^{(\alpha a)}$, and n_1 are viewed as adjustable parameters. Then, the constitutive relation for the (αa)th slip system is given by

$$\tau^{(\alpha a)} = \operatorname{sgn}(\dot\gamma^{(\alpha a)})\left\{\tau_{\mathrm{a0}}^{(\alpha a)} + \tau_{\mathrm{a1}}^{(\alpha a)}(\gamma^{(\alpha a)})^{n_1} + \hat\tau_0^{(\alpha a)}[1 + a^{(\alpha a)}(T)(\gamma_{\mathrm{I}}^{(\alpha a)})^{n_0}]\right\}\left[1 - \left(-\frac{kT}{G_0^{(\alpha a)}} \times \ln\frac{\left|\dot\gamma^{(\alpha a)}\right|[1 + a^{(\alpha a)}(T)(\gamma_{\mathrm{I}}^{(\alpha a)})^{n_0}]}{\dot\gamma_0^{(\alpha a)}}\right)^{1/q}\right]^{1/p}\Bigg\}$$

for $T \leqslant T_{\mathrm{c}}^{(\alpha a)}$ (3.21a)

and

$$\tau^{(\alpha a)} = \operatorname{sgn}(\dot\gamma^{(\alpha a)})[\tau_{a0}^{(\alpha a)} + \tau_{a1}^{(\alpha a)}(\gamma^{(\alpha a)})^{n_1}] \quad \text{for } T > T_{\mathrm{c}}^{(\alpha a)}, \tag{3.21b}$$

where, again,

$$\dot\gamma_0^{(\alpha a)} \equiv b^{(\alpha a)}\rho_{\mathrm{m}}^{(\alpha a)}\omega_0^{(\alpha a)} l_0^{(\alpha a)}, \tag{3.21c}$$

$$\hat\tau_0^{(\alpha a)} = G_0^{(\alpha a)}/[b^{(\alpha a)}\lambda^{(\alpha a)} l_0^{(\alpha a)}], \tag{3.21d}$$

$$a^{(\alpha a)}(T) = a_0^{(\alpha a)}[1 - (T/T_{\mathrm{m}})^2], \tag{3.21e}$$

and the critical temperature, $T_{\mathrm{c}}^{(\alpha a)}$, is determined by

$$T_{\mathrm{c}}^{(\alpha a)} = -G_0^{(\alpha a)}/\{k\ln[|\dot\gamma^{(\alpha a)}| \times (1 + a^{(\alpha a)}(T_{\mathrm{c}}^{(\alpha a)})(\gamma_{\mathrm{I}}^{(\alpha a)})^{n_0})/\dot\gamma_{\mathrm{r}}^{(\alpha a)}]\}. \tag{3.21f}$$

The plastic strain rate for the (αa)th slip system is given by

$$\dot\gamma^{(\alpha a)} = \frac{\operatorname{sgn}(\tau^{(\alpha a)})\dot\gamma_0^{(\alpha a)}}{1 + a^{(\alpha a)}(T)[\gamma_{\mathrm{I}}^{(\alpha a)}]^{n_0}} \times \exp\left[-\frac{G_0^{(\alpha a)}}{kT}\left\{1 - \left(\frac{|\tau^{(\alpha a)}| - \tau_{\mathrm{a}}^{(\alpha a)}}{\hat\tau_0^{(\alpha a)}[1 + a^{(\alpha a)}(T)(\gamma_{\mathrm{I}}^{(\alpha a)})^{n_0}]}\right)^p\right\}^q\right],$$

when $|\tau^{(\alpha a)}| \geqslant \tau_{\mathrm{a}}^{(\alpha a)}$, (3.22a)

$$\dot\gamma^{(\alpha a)} = 0 \quad \text{otherwise.} \tag{3.22b}$$

We assume that the increment of temperature is proportional to the increment of the plastic work, so that the temperature, T, is given by

$$T = T_0 + \eta\Delta w^{\mathrm{p}}, \tag{3.23}$$

where Δw^{p} is the increment of the plastic work, and η the conversion factor, including a factor which defines the portion of the plastic work used to heat the material. For a single fcc crystal, the increment of the plastic work, Δw^{p}, can be calculated by

$$\Delta w^{\mathrm{p}} = \sum_{\alpha=1}^{4}\sum_{a=1}^{3}\int_0^{\gamma^{(\alpha a)}} \tau^{(\alpha a)}\,\mathrm{d}\gamma^{(\alpha a)}. \tag{3.24}$$

For an fcc polycrystal, the calculation for the temperature will be discussed in the forthcoming section.

3.4. Fcc versus bcc crystals

As explained before, the primary barriers to the motion of dislocations in fcc and bcc crystals are essentially different: the dominant barriers in fcc crystals are the dislocation forests which intersect the slip plane, whereas those in bcc crystals are the Peierls lattice stresses. For fcc crystals, the energy required to cross the Peierls barrier is generally small (less than 0.2 eV), and only at very low

temperatures the Peierls barrier becomes important. For bcc crystals, the average spacing of the barriers, $d^{(\alpha a)}$, equals the magnitude of the Burgers vector, $b^{(\alpha a)}$, which is a constant, and $l^{(\alpha a)} = l_0^{(\alpha a)} = b^{(\alpha a)}$ is also a constant. Then in the constitutive relation Eqs. (3.21a)–(3.21f), for bcc crystals, $a_0^{(\alpha a)} \equiv a_0 = 0$, $f = 1$, and

$$\hat{\tau}^{(\alpha a)} = \hat{\tau}_0^{(\alpha a)} = G_0^{(\alpha a)}/[(b^{(\alpha a)})^2 \lambda^{(\alpha a)}], \tag{3.25a}$$

$$\dot{\gamma}_{\mathrm{r}}^{(\alpha a)} = \dot{\gamma}_0^{(\alpha a)} = \rho_{\mathrm{m}}^{(\alpha a)} \omega_0^{(\alpha a)} [b^{(\alpha a)}]^2. \tag{3.25b}$$

In the case of fcc crystals, on the other hand, the intersecting dislocations are the barriers. The core of a dislocation involves several surrounding atoms. Therefore, the magnitude of the energy barrier is expected to be considerably greater than the lattice resistance. Thus, the constitutive parameter $k/G_0^{(\alpha a)}$, for fcc OFHC copper is estimated to be 4.9×10^{-5} K^{-1} by Nemat-Nasser and Li (1998), which is about half of the value estimated for bcc tantalum, 8.62×10^{-5} K^{-1}, by Nemat-Nasser and Isaacs (1997). We use the same value of $k/G_0^{(\alpha a)} = 4.9 \times 10^{-5}$ K^{-1} in our crystal plasticity model calculations for fcc OFHC copper.

3.5. Annealed versus as-received fcc samples

The initial average dislocation (barrier) spacing for annealed fcc samples is expected to be greater than that for the as-received samples. Hence, from Eq. (3.12b), the value of $\hat{\tau}_0^{(\alpha a)}$ for annealed samples is expected to be smaller than that for the as-received samples. The parameter $a_0^{(\alpha a)}$ in Eq. (3.11a), is also expected to be greater for the annealed samples than that for the as-received ones. For the continuum model of OFHC copper, Nemat-Nasser and Li (1998) choose $a_0^{(\alpha a)} \equiv a_0 = 20$ for the annealed samples, and $a_0^{(\alpha a)} \equiv a_0 = 1.8$ for the as-received samples. In our crystal plasticity model calculation for fcc OFHC copper, we also assume $a_0^{(\alpha a)} = a_0$, for all the slip systems, and use those same values of a_0 as used for the continuum model in Nemat-Nasser and Li (1998). In view of Eq. (3.13b), $\dot{\gamma}_0^{(\alpha a)}$ depends on the initial dislocation spacing, $l_0^{(\alpha a)}$. As is seen, $\dot{\gamma}_0^{(\alpha a)}$ also depends on the density of the mobile dislocations, $\rho_{\mathrm{m}}^{(\alpha a)}$, and the frequency, $\omega_0^{(\alpha a)}$, both of which are affected by $l_0^{(\alpha a)}$. We assume that the product $\rho_{\mathrm{m}}^{(\alpha a)} \omega_0^{(\alpha a)} l_0^{(\alpha a)}$ remains essentially the same whether the sample is annealed or not. This may be a crude approximation, but it seems to be adequate for the present application.

4. Computational algorithm

Nemat-Nasser and Okinaka (1996) have proposed an efficient computational method for fcc crystals, which is based on the *plastic-predictor, elastic-corrector* method, combined with the conventional forward-gradient technique. In their calculation, the rate-dependent slip model with the power-law is used. In a recent work, Nemat-Nasser et al. (1998) successfully employed this method to solve finite-deformation problems of bcc single- and poly-crystals, using the physically based constitutive model of Nemat-Nasser (1996). In the present work, we apply a similar computational strategy to the fcc crystal calculation, using the fcc crystal constitutive model described in Section 3.

Consider an fcc polycrystal which is composed of M single crystals. Assume that all the grains have the same volume, and that the initial orientations of the crystals are uniformly distributed. The Taylor averaging method is employed, i.e., it is assumed that each grain of the polycrystal undergoes the same deformation and deformation rate. Hence, in all grains, $\boldsymbol{L} = \bar{\boldsymbol{L}}$, where $\boldsymbol{L}$ and $\bar{\boldsymbol{L}}$ denote the local and overall velocity gradients, respectively. The equivalent plastic strain rate and the equivalent stress of the polycrystal must be calculated by averaging over all the grains. The overall temperature is then computed using the average equivalent plastic strain rate and stress.

4.1. Single crystals

As discussed in Nemat-Nasser and Okinaka (1996), for each single crystal, the material deformation history can be divided into three regimes according to the number of active slip systems. A slip system is called active, if its resolved shear stress satisfies $|\tau^{(\alpha a)}| \geqslant \tau_{\mathrm{a}}^{(\alpha a)}$. From the constitutive relation Eq. (3.22a), $\dot{\gamma}^{(\alpha a)} = 0$ for the non-active slip system. Denoting the number of active systems in the single crystal by N, the three regimes are:

1. Rapidly-changing regime: elastic deformation plays an important role;
2. Transition regime: $0 < N \leqslant 5$;
3. Steady-state regime: $N > 5$.

When a material is in the transition regime, the resolved shear stresses may increase with time, leading to activation of additional slip systems. When the loading starts, or the loading conditions are suddenly changed, then the elastic deformation plays an essential role, and the material is in the rapidly-changing regime.

All the solutions are obtained incrementally. Different numerical methods are applied for different regimes. For the transition and the steady-state regimes, the plastic-predictor, elastic-corrector method is used. This starts with the tentative assumption that the total deformation increment is solely due to plastic slip, and then corrects the results by including the accompanying elastic contribution. Since, in general, the elastic contribution is much smaller than the plastic one, the method efficiently yields accurate results. Indeed, in many cases, the slip rate due to elastic distortion (but not the associated stress rate) may be neglected in the transition and steady-state regimes. In the rapidly changing regime, the explicit Euler method is employed.

4.2. Polycrystals

For the calculation of each crystal, it is necessary to use two different time increments, depending on the deformation regime. The time increment for the explicit Euler method is much smaller than that for the plastic-predictor, elastic-corrector method. The time increments are thus, in general, not uniform for all grains. Hence, in the calculation of the polycrystal, it is necessary to assign a *time period*, Δt^{av}, at the end of which the averaging to obtain polycrystal properties is performed. Define the averaging time intervals by $[t^{\mathrm{av}}_{j-1}, t^{\mathrm{av}}_j]$, $j = 1, 2, \ldots, J$, where

$$t^{\mathrm{av}}_0 = 0 \tag{4.1a}$$

is the beginning of the model calculation, and

$$t^{\mathrm{av}}_j = t^{\mathrm{av}}_{j-1} + \Delta t^{\mathrm{av}}, \quad j = 1, 2, \ldots, J \tag{4.1b}$$

stand for the end of the jth averaging interval; J is the total number of times when the averaging is performed. At the end of each averaging interval, t^{av}_j, $j = 1, 2, .., J$, the equivalent overall plastic strain rate and the equivalent stress of the polycrystal are obtained by averaging over all grains. The overall temperature is calculated from the average plastic work rate per unit volume. This average work rate is assumed to remain unchanged within each averaging time interval.

Noting that all the grains have the same volume, the volume average of the Cauchy stress at the end of the averaging interval, t^{av}_j, $j = 1, 2, \ldots, J$, is given by

$$\boldsymbol{\Sigma}(t^{\mathrm{av}}_j) = \frac{1}{V}\int_V \boldsymbol{\sigma}(t^{\mathrm{av}}_j)\,\mathrm{d}V = \frac{1}{M}\sum_{n=1}^{M}\boldsymbol{\sigma}_n(t^{\mathrm{av}}_j), \tag{4.2a}$$

where M is the number of grains and $\boldsymbol{\sigma}_n$ the Cauchy stress for the nth grain of the polycrystal. The equivalent stress, $\Sigma_{\mathrm{eq}}(t^{\mathrm{av}}_j)$, is then calculated as

$$\Sigma_{\mathrm{eq}}(t^{\mathrm{av}}_j) = (3/2\boldsymbol{\Sigma}(t^{\mathrm{av}}_j) : \boldsymbol{\Sigma}(t^{\mathrm{av}}_j))^{1/2}. \tag{4.2b}$$

The plastic part of the strain rate for the nth grain of the polycrystal is given by

$$\boldsymbol{D}^{\mathrm{p}}_n = \sum_{\alpha=1}^{4}\sum_{a=1}^{3}\dot{\gamma}^{(\alpha a)}_n \boldsymbol{p}^{(\alpha a)}_n, \tag{4.3}$$

where $n = 1, \ldots, M$ are the grain indices. The volume average of the plastic strain rate, $\bar{\boldsymbol{D}}^{\mathrm{p}}$, and the equivalent plastic strain rate, $\dot{\gamma}_{\mathrm{eq}}$, at t^{av}_j, $j = 1, 2, \ldots, J$, are defined by

$$\bar{\boldsymbol{D}}^{\mathrm{p}}(t^{\mathrm{av}}_j) = \frac{1}{M}\sum_{n=1}^{M}\boldsymbol{D}^{\mathrm{p}}_n(t^{\mathrm{av}}_j) \tag{4.4a}$$

and

$$\dot{\gamma}_{\mathrm{eq}}(t^{\mathrm{av}}_j) = (2/3\bar{\boldsymbol{D}}^{\mathrm{p}}(t^{\mathrm{av}}_j) : \bar{\boldsymbol{D}}^{\mathrm{p}}(t^{\mathrm{av}}_j))^{1/2}, \tag{4.4b}$$

respectively.

The plastic work rate per unit volume is approximated by

$$\dot{W}^{\mathrm{p}}(t^{\mathrm{av}}_j) \approx \Sigma_{\mathrm{eq}}(t^{\mathrm{av}}_j)\dot{\gamma}_{\mathrm{eq}}(t^{\mathrm{av}}_j). \tag{4.5a}$$

The approximate temperature of the polycrystal material element (the test sample) is calculated from

$$T_{\mathrm{A}}(t) = T(t^{\mathrm{av}}_{j-1}) + \eta\dot{W}^{\mathrm{p}}(t^{\mathrm{av}}_{j-1})[t - t^{\mathrm{av}}_{j-1}], \tag{4.5b}$$

where t is in the jth averaging interval and satisfies $t_{j-1}^{\mathrm{av}} < t \leqslant t_j^{\mathrm{av}}$. Again, the conversion factor η includes a factor which defines the fraction of the plastic work converted into heat.

4.3. Main equations

To introduce the main equations for the computational algorithm in each single crystal, note that

$$\tau^{(\alpha a)} = \boldsymbol{\sigma} : \boldsymbol{p}^{(\alpha a)}, \tag{4.6}$$

where $\tau^{(\alpha a)}$ is the resolved shear stress and $\boldsymbol{\sigma}$ is the Cauchy stress. Take the time derivative of both sides of Eq. (4.6) to obtain

$$\dot{\tau}^{(\alpha a)} = \dot{\boldsymbol{\sigma}} : \boldsymbol{p}^{(\alpha a)} + \boldsymbol{\sigma} : \dot{\boldsymbol{p}}^{(\alpha a)}. \tag{4.7}$$

Noting that

$$\dot{\boldsymbol{p}}^{(\alpha a)} = \boldsymbol{\Omega}^* \boldsymbol{p}^{(\alpha a)} - \boldsymbol{p}^{(\alpha a)} \boldsymbol{\Omega}^*, \tag{4.8a}$$

from Eq. (4.7) obtain

$$\begin{aligned} \dot{\tau}^{(\alpha a)} &= (\dot{\boldsymbol{\sigma}} - \boldsymbol{\Omega}^* \boldsymbol{\sigma} + \boldsymbol{\sigma} \Omega^*) : \boldsymbol{p}^{(\alpha a)} \equiv \overset{o}{\boldsymbol{\sigma}} : \boldsymbol{p}^{(\alpha a)} \\ &= \boldsymbol{C}^* : \boldsymbol{D}^* : \boldsymbol{p}^{(\alpha a)}, \end{aligned} \tag{4.8b}$$

where $\overset{o}{\boldsymbol{\sigma}} \equiv \dot{\boldsymbol{\sigma}} - \boldsymbol{\Omega}^* \boldsymbol{\sigma} + \boldsymbol{\sigma} \boldsymbol{\Omega}^*$ is the Jamman rate of the Cauchy stress, and the elasticity relation $\overset{o}{\boldsymbol{\sigma}} = \boldsymbol{C}^* : \boldsymbol{D}^*$ is used (see, e.g., Nemat-Nasser and Okinaka, 1996; or Nemat-Nasser, 1998).Consider now the inner product of the total deformation rate, $\boldsymbol{D}$, (2.8a), with the symmetric part of the rotated slip-system tensor, $\boldsymbol{p}^{(\alpha a)}$, and using Eq. (4.8b) obtain

$$\boldsymbol{p}^{(\alpha a)} : \mathscr{L} : \boldsymbol{D} = \frac{1}{2\mu} \dot{\tau}^{(\alpha a)} + \sum_{\beta=1}^{4} \sum_{b=1}^{3} H_{(\beta b)}^{(\alpha a)} \dot{\gamma}^{(\beta b)}, \tag{4.9a}$$

where

$$H_{(\beta b)}^{(\alpha a)} = \boldsymbol{p}^{(\beta b)} : \mathscr{L} : \boldsymbol{p}^{(\alpha a)} \tag{4.9b}$$

and

$$\dot{\tau}^{(\alpha a)} = 2\mu \boldsymbol{D}^* : \mathscr{L} : \boldsymbol{p}^{(\alpha a)}, \tag{4.9c}$$

here $\boldsymbol{C}^* = 2\mu\, \mathscr{L}$ is the elasticity tensor, and μ a shear modulus used here to render the tensor $\mathscr{L}$ dimensionless; to simplify the crystal plasticity model calculation, we assume that the material is elastically isotropic; $\mathscr{L}$ is then a fourth-order symmetric identity tensor.

4.4. Algorithm

The calculation proceeds incrementally. Denote by t_0 the beginning of the time step, and by Δt the time increment. Given a constant $\boldsymbol{D}$ over a time increment Δt, the increments $\Delta\tau^{(\alpha a)}$'s and $\Delta\gamma^{(\alpha a)}$'s are to be calculated from Eq. (4.9a). For the Euler method, the increments $\Delta\tau^{(\alpha a)}$'s are first obtained, then the resolved shear stresses, $\tau^{(\alpha a)}$, and the slip rates, $\dot{\gamma}^{(\alpha a)}$, are updated.

In the plastic-predictor technique, it is assumed that the stable condition, $\dot{\tau}^{(\alpha a)} \approx 0$, is satisfied in all active slip systems. With this assumption and for elastically isotropic case, (4.9a) becomes

$$\boldsymbol{D} : \boldsymbol{p}^{(\alpha a)} = \sum_{(\beta b)} H_{(\beta b)}^{(\alpha a)} \dot{\gamma}_{\mathrm{A}}^{(\beta b)}, \tag{4.10}$$

where the subscript A stands for the *approximate* value.

Observe that only five of the symmetric slip-system tensors, $\boldsymbol{p}^{(\alpha a)}$'s, are linearly independent, as discussed in Section 2 Hence, in the transition regime, where the number of active slip systems is not greater than 5, the matrix $\boldsymbol{H}$ is non-singular. In that case, from the linear system (4.10), $\dot{\gamma}_{\mathrm{A}}^{(\alpha a)}$'s can be uniquely obtained. However, in the steady-state regime, where the number of active slip systems is more than five, $\boldsymbol{H}$ is singular. In such a case, this system of linear equations must be supplemented by equations representing the interdependency of the resolved shear stresses. From Eq. (4.6) and the interdependency relations (2.9a)–(2.9d) and (2.10a)–(2.10c), the following interdependency relations for the resolved shear stresses are obtained:

$$\begin{aligned} &\tau^{(11)} + \tau^{(12)} + \tau^{(13)} = 0, \\ &\tau^{(21)} + \tau^{(22)} + \tau^{(23)} = 0, \end{aligned} \tag{4.11a}$$

$$\begin{aligned} &\tau^{(31)} + \tau^{(32)} + \tau^{(33)} = 0, \\ &\tau^{(41)} + \tau^{(42)} + \tau^{(43)} = 0, \end{aligned} \tag{4.11b}$$

$$\begin{aligned} &-\tau^{(11)} + \tau^{(22)} + \tau^{(43)} = 0, \\ &-\tau^{(12)} - \tau^{(33)} + \tau^{(41)} = 0, \end{aligned} \tag{4.11c}$$

$$\tau^{(13)} - \tau^{(21)} + \tau^{(32)} = 0. \tag{4.11d}$$

Since the calculation is incremental, the active slip systems are known at the beginning of each in-

crement. Hence, the 12 conditions can be reduced to include only the active slip systems. The reduced $N-5$ conditions are then chosen and collectively written in matrix form, as

$$\sum_{(\alpha a)} M_i^{(\alpha a)} \tau^{(\alpha a)} = 0, \tag{4.12a}$$

where $1 \leqslant i \leqslant N-5$ and the summation is performed over all active slip systems. These equations, in their incremental forms,

$$\sum_{(\alpha a)} M_i^{(\alpha a)} \Delta\tau^{(\alpha a)} = 0, \tag{4.12b}$$

together with Eq. (4.10), are used to obtain the first estimate of the slip rates.

To simplify the calculation, the following approximations are used. First, assume that the plastic strain, $\gamma_{\mathrm{I}}^{(\alpha a)}$, produced by slips on the intersecting slip planes, is approximately equal to the calculated total plastic strain, $\gamma^{(\alpha a)}$, leading to

$$\gamma_{\mathrm{I}}^{(\alpha a)} \approx \gamma^{(\alpha a)} = \sum_{\beta=1}^{4}\sum_{b=1}^{3} K_{(\beta b)}^{(\alpha a)} \int_0^t \left|\dot\gamma^{(\beta b)}(\xi)\right| \mathrm{d}\xi. \tag{4.13a}$$

Second, assume that all $K_{(\beta b)}^{(\alpha a)}$ are the same and are absorbed into the corresponding adjustable parameters $a_0^{(\alpha a)}$ and $\tau_{\mathrm{a1}}^{(\alpha a)}$. This leads to

$$\gamma_{\mathrm{I}}^{(\alpha a)} = \gamma^{(\alpha a)} \equiv \gamma, \tag{4.13b}$$

for all slip systems. Finally, as in Eqs. (3.11a) and (3.11b), consider

$$f(\gamma_{\mathrm{I}}^{(\alpha a)}, T) = 1 + a^{(\alpha a)}(T)\gamma_{\mathrm{I}}^{n_0} \approx 1 + a^{(\alpha a)}(T)\gamma^{n_0}, \tag{4.14a}$$

$$a^{(\alpha a)}(T) = a_0^{(\alpha a)}[1 - (T/T_{\mathrm{m}})^2] \tag{4.14b}$$

and assume that $n_0 = 1/2$ and $a_0^{(\alpha a)} = a_0$ are constants for all slip system, arriving at

$$f = 1 + a_0[1 - (T/T_{\mathrm{m}})^2]\gamma^{1/2}. \tag{4.14c}$$

While these simplifying assumptions seem crude, they are adequate for our application.

Differentiating both sides of Eqs. (3.21a) and (3.21b), using $p = 2/3$ and $q = 2$ as suggested by Ono (1968), the shear-stress increments, $\Delta\tau^{(\alpha a)}$, are expressed as

$$\Delta\tau^{(\alpha a)} = H_1^{(\alpha a)}\Delta\gamma + H_2^{(\alpha a)}\Delta T + H_3^{(\alpha a)}\Delta\dot\gamma^{(\alpha a)}, \tag{4.15}$$

where $H_i^{(\alpha a)}$, for $i = 1, 2, 3$, evaluated at t_0, are explicitly given as follows:

$$H_1^{(\alpha a)} \equiv n_1 \tau_0^{(\alpha a)} \gamma^{n_1 - 1} + \frac{3kT\hat\tau_0^{(\alpha a)} a(T)}{8G_0\gamma^{1/2}} \left(\frac{1 - X^{1/2}}{X}\right)^{1/2} + \frac{\hat\tau_0^{(\alpha a)} a(T)}{2\gamma^{1/2}}(1 - X^{1/2})^{3/2}, \tag{4.16}$$

$$H_2^{(\alpha a)} \equiv \frac{3k\hat\tau^{(\alpha a)}}{4G_0} \times \ln[|\dot\gamma^{(\alpha a)}|(1 + a(T)\gamma^{1/2})/\dot\gamma_0^{(\alpha a)}] \left(\frac{1 - X^{1/2}}{X}\right)^{1/2} - \frac{3k\hat\tau_0 a_0 T^2 \gamma^{1/2}}{2G_0 T_{\mathrm{m}}^2} \left(\frac{1 - X^{1/2}}{X}\right)^{1/2} - \frac{2\hat\tau_0 a_0 T\gamma^{1/2}}{T_{\mathrm{m}}^2}(1 - X^{1/2})^{3/2} \tag{4.17}$$

and

$$H_3^{(\alpha a)} \equiv \frac{3kT\hat\tau^{(\alpha a)}}{4G_0\dot\gamma^{1/2}} \left(\frac{1 - X^{1/2}}{X}\right)^{1/2}, \tag{4.18}$$

where $\hat\tau^{(\alpha a)}$ is defined in Eq. (3.19), and X is given by

$$X \equiv -(kT/G_0^{(\alpha a)}) \ln[|\dot\gamma^{(\alpha a)}|(1 + a(T)\gamma^{1/2})/\dot\gamma_0^{(\alpha a)}] \quad \text{for } T \leqslant T_{\mathrm{c}}^{(\alpha a)},$$

$$X \equiv 1 \text{ for } T > T_{\mathrm{c}}^{(\alpha a)}, \tag{4.19}$$

with the critical temperature $T_{\mathrm{c}}^{(\alpha a)}$ defined in (3) with $n_0 = 1/2$. As stated before, in calculating $H_i^{(\alpha a)}$, for $i = 1, 2, 3$, X, the quantities $\hat\tau^{(\alpha a)}$ and γ, and the temperature of the polycrystal, T, are all evaluated at t_0. In (4.15), we approximate values of $\Delta\gamma$, $\Delta\dot\gamma^{(\alpha a)}$, and ΔT, respectively, by

$$\Delta\gamma_{\mathrm{A}} = \sum_{\alpha a=1}^{N} \mathrm{sgn}(\dot\gamma^{(\alpha a)}(t_0)) \times [(1-\theta)\dot\gamma_{\mathrm{A}}^{(\alpha a)} + \theta\dot\gamma^{(\alpha a)}(t_0)]\Delta t, \tag{4.20}$$

$$\Delta\dot\gamma_{\mathrm{A}}^{(\alpha a)} = \dot\gamma_{\mathrm{A}}^{(\alpha a)} - \dot\gamma^{(\alpha a)}(t_0), \tag{4.21}$$

$$\Delta T_{\mathrm{A}} = \eta\dot W^{\mathrm{p}}(t_{j-1}^{\mathrm{av}})\Delta t, \tag{4.22}$$

when t_0 is in the jth averaging interval and satisfies $t_{j-1}^{\mathrm{av}} \leqslant t_0 < t_j^{\mathrm{av}}$; again a subscript A describes the corresponding approximate value. This yields

$$\Delta\tau^{(\alpha a)} = \sum_{(\beta b)} P_{(\beta b)}^{(\alpha a)} \dot{\gamma}_A^{(\beta b)} + q^{(\alpha a)}, \tag{4.23a}$$

where

$$P_{(\beta b)}^{(\alpha a)} = \operatorname{sgn}(\dot{\gamma}^{(\beta b)}(t_0))(1-\theta)\Delta t H_1^{(\alpha a)} + \delta_{(\beta b)}^{(\alpha a)} H_3^{(\alpha a)}, \tag{4.23b}$$

$$q^{(\alpha a)} = \eta \dot{W}^{\mathrm{p}}(t_L) H_2^{(\alpha a)} + \sum_{(\beta b)} \{\theta \Delta t \operatorname{sgn}(\dot{\gamma}^{(\beta b)}(t_0)) H_1^{(\alpha a)} - \delta_{(\beta b)}^{(\alpha a)} H_3^{(\alpha a)}\} \dot{\gamma}^{(\beta b)}(t_0). \tag{4.23c}$$

Here, $\delta_{(\beta b)}^{(\alpha a)}$ is the Kronecker symbol defined by

$$\delta_{(\beta b)}^{(\alpha a)} = \begin{cases} 1 & \beta = \alpha \text{ and } b = a, \\ 0 & \text{otherwise} \end{cases} \tag{4.23d}$$

and $\{P_{(\beta b)}^{(\alpha a)}\}$ is an $N \times N$ matrix.

Substitute Eq. (4.23a) into Eq. (4.12b) to obtain the following $N-5$ equations for approximate slip rates $\dot{\gamma}_{\mathrm{A}}^{(\beta)}$:

$$\sum_{(\alpha a)} M_i^{(\alpha a)} \left(\sum_{(\beta b)} P_{(\beta b)}^{(\alpha a)} \dot{\gamma}_{\mathrm{A}}^{(\beta b)} + q^{(\alpha a)} \right) = 0 \tag{4.24}$$

Expression Eq. (4.24) together with Eq. (4.10) form N linear equations for N unknowns, which are then solved to give the approximate slip rates $\dot{\gamma}_A^{(\alpha a)}$'s. Here, we omit the elastic corrector procedure, since the obtained approximate slip rates are, in general, already sufficiently accurate, although they can be further improved by including the elastic correction in the same manner as discussed by Nemat-Nasser and Okinaka (1996).

Using the approximate slip rates in Eqs. (4.20) and (4.22), the plastic strain and the temperature are now updated by

$$\gamma_{\mathrm{A}} = \gamma(t_0) + \Delta\gamma_{\mathrm{A}} \tag{4.25a}$$

and

$$T_{\mathrm{A}} = T(t_0) + \Delta T_{\mathrm{A}}, \tag{4.25b}$$

respectively. The athermal components of the resolved shear stresses are calculated from

$$\tau_{\mathrm{a}A}^{(\alpha a)} = \tau_{\mathrm{a}0}^{(\alpha a)} + \tau_{\mathrm{a}1}^{(\alpha a)} \gamma_{\mathrm{A}}^{n_1}. \tag{4.26}$$

The shear stresses are then obtained from the constitutive relation Eqs. (3.21a) and (3.21b).

To obtain the approximate updated rigid-body rotation for each single crystal, we first use the mean value theorem to write

$$\begin{aligned} \boldsymbol{R}^*(t_0+\Delta t) &= \boldsymbol{R}^*(t_0) + \dot{\boldsymbol{R}}^*(t_0+s\Delta t)\Delta t \\ &= [1 + \dot{\boldsymbol{R}}^*(t_0+s\Delta t)\boldsymbol{R}^{*\mathrm{T}}\Delta t]\boldsymbol{R}(t_0), \end{aligned} \tag{4.27}$$

where $0 \leqslant s \leqslant 1$. Then, we approximate $\dot{\boldsymbol{R}}^*(t_0 + s\Delta t)\boldsymbol{R}^{*\mathrm{T}}$ by $\theta\Omega^*(t_0) + (1-\theta)\Omega_A^*$, where Ω_A^* is calculated from (2.8b), using the approximate updated values of the slip rates $\dot{\gamma}_{\mathrm{A}}^{(\alpha a)}$'s.

The updated Cauchy stress is then obtained from the approximate resolved shear stresses, $\tau_{\mathrm{A}}^{(\alpha a)}$, by choosing five independent slip system tensors, $\boldsymbol{p}^{(\alpha a)}$, and solving the system of linear equations corresponding to Eq. (4.6) for the stress components.

5. Comparison with experimental results

Extensive experimental data on commercially pure OFHC copper have been reported recently by Nemat-Nasser and Li (1998). These experiments cover a broad range of strain rates (0.001–$8 \times 10^3\ s^{-1}$) and temperatures (77–1096 K), with strains close to 100% for both the as-received and annealed samples.

To obtain the overall strain rates used in the compression tests, in our model calculations, the constant overall velocity gradient is taken to be

$$\bar{\boldsymbol{L}} = \begin{bmatrix} \dot{\gamma}_{\mathrm{eq}} & 0 & 0 \\ 0 & -\frac{1}{2}\dot{\gamma}_{\mathrm{eq}} & 0 \\ 0 & 0 & -\frac{1}{2}\dot{\gamma}_{\mathrm{eq}} \end{bmatrix} (s^{-1}), \tag{5.1a}$$

where $\dot{\gamma}_{\mathrm{eq}}$ is set equal to the imposed uniaxial strain rate, in the compression Hopkinson bar or in the quasi-static testing machine. This yields

$$\dot{\gamma}_{\mathrm{eq}} = (2/3\boldsymbol{D} : \boldsymbol{D})^{1/2}. \tag{5.1b}$$

5.1. Estimate of parameters

As discussed in Nemat-Nasser et al. (1998), at high strain rates, essentially all the heat generated

Table 2
Values of the constitutive parameters which are common to continuum and crystal plasticity models

	p	q	k/G_0 (K^{-1})	$\dot{\gamma}_0$ (s^{-1})	τ_{a0}	a_0	n_0	n_1
Annealed copper	2/3	2	4.9×10^{-5}	2×10^{10}	0	20	0.5	0.3
As-received copper	2/3	2	4.9×10^{-5}	2×10^{10}	0	1.8	0.5	0.3

by the plastic deformation is used to increase the sample temperature; see also Kapoor and Nemat-Nasser (1998). In what follows, we have thus assumed that 100% of the plastic work, which correspond to the conversion factor $\eta = 0.433$ (when stress is measured in MPa and temperature in K), is used to increase the temperature of the sample. The time increment is adjusted to allow a 1% increment of the equivalent strain in the plastic-predictor method, whereas a 0.001% increment of the equivalent strain is used for the explicit Euler method. The time period Δt^{av}, at the end of which the averaging is performed, is taken to correspond to a 1% of the equivalent strain, which, hence, is variable. Therefore, at every 1% of the equivalent strain, the polycrystal properties are obtained by averaging over all grains.

In our simulations, for simplicity, the values of all parameters are taken to be the same for all slip systems. We consider only the stresses $\hat{\tau}_0^{(\alpha a)} = \hat{\tau}_0$ and $\tau_0^{(\alpha a)} = \tau_0$ as the adjustable parameters which may depend on the specific material. The values of all the remaining constitutive parameters are taken to be the same as those estimated by Nemat-Nasser and Li (1998) in their continuum model. These parameters are: $k/G_0^{(\alpha a)} = 4.9 \times 10^{-5}\ K^{-1}$, $\dot{\gamma}_0^{(\alpha a)} = 2 \times 10^{10}\ s^{-1}$, $\tau_{a0}^{(\alpha a)} = \tau_{a0} = 0$, $a_0 = 20$ for annealed copper; and $a_0 = 1.8$ for as-received copper, $n_0 = 0.5$, $n_1 = 0.3$, $p = 2/3$, and $q = 2$, which are listed in Table 2.

In our model calculation, the two adjustable parameters for both the as-received and annealed cases are determined to best simulate the experimental data. For the annealed case,

$$\hat{\tau}_0 = 9\ \text{MPa}, \quad \tau_0 = 50\ \text{MPa},$$

and for the as-received case,

$$\hat{\tau}_0 = 95\ \text{MPa}, \quad \tau_0 = 48\ \text{MPa},$$

which are summarized in Table 3.

These parameters uniformly fit all the experimental data for the temperature from 77 to 1096 K and the strain rate 4000 s^{-1}; temperatures of 77 K and the strain rate 8000 s^{-1}; and temperature 296 K and the strain rates of 8000, 0.1, and 0.001 s^{-1}. The results are in remarkably good agreement with the experimental data and those of the continuum model calculations.

5.2. Comparison

The comparison between the results of the equivalent stress obtained by the experiments, the continuum model calculation, and the new crystal plasticity model calculation at a 4000 s^{-1} strain rate and initial temperatures of 77, 496, 696, 896, and 1096 K for annealed and as-received OFHC copper is presented in Figs. 1 and 2, respectively. The comparison for a 4000 s^{-1} strain rate and initial temperatures of 296, 596, 796, and 996 K for annealed and as-received OFHC copper is given in Figs. 3 and 4, respectively.

The comparison between the results of the equivalent stress obtained by the experiments, the continuum model calculation, and the new crystal plasticity model calculation at a 8000 s^{-1} strain rate and temperatures of 77 K and 296 K, and at a 296 K temperature and strain rates of 8000, 0.1,

Table 3
Values of the two adjustable constitutive parameters which are different for the continuum model and the crystal plasticity model

	$\hat{\tau}_0$ (MPa)	τ_{a1} (MPa)
Annealed copper		
Crystal Plasticity Model	9	50
Continuum Model	46	220
As-received copper		
Crystal Plasticity Model	95	48
Continuum Model	400	220

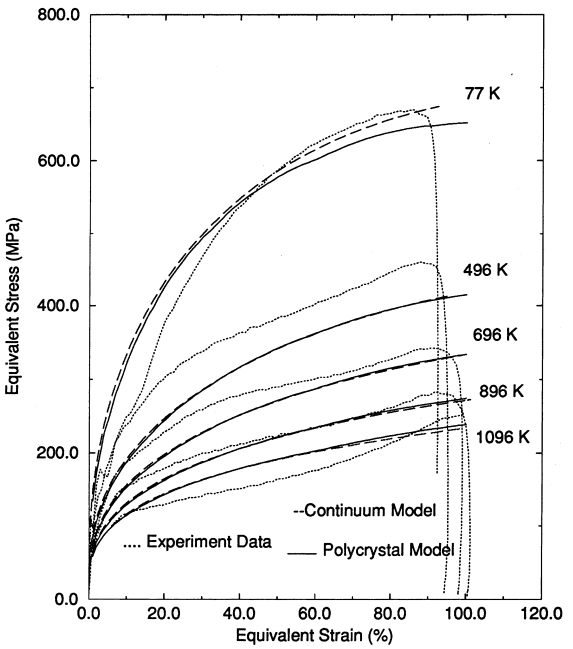

Fig. 1. Comparison between the experimental data, the continuum model calculation, and the crystal plasticity model calculation for polycrystalline annealed OFHC copper at 4000 s^{-1} strain rate and initial temperatures of 77, 496, 696, 896, and 1096 K. Dotted curves represent the experimental data, long dash curves represent the continuum model calculation, and solid curves are the model calculation using the new crystal plasticity constitutive model, the proposed algorithm, and the Taylor averaging method.

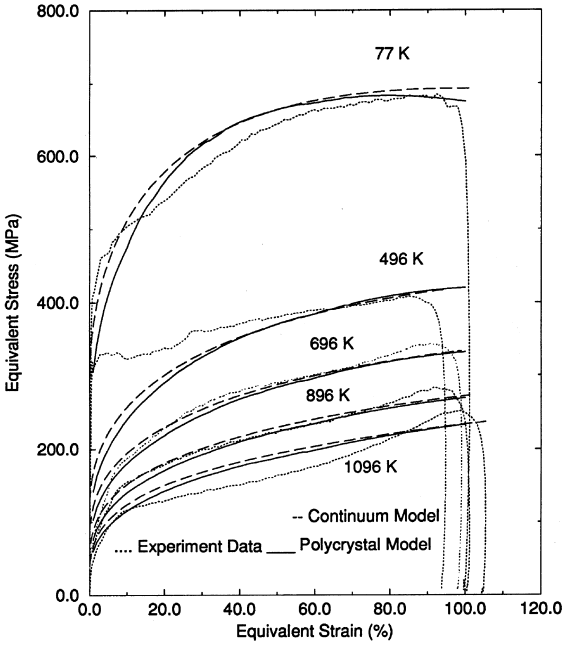

Fig. 2. Comparison between the experimental data, the continuum model calculation, and the crystal plasticity model calculation for polycrystalline as-received OFHC copper at 4000 s^{-1} strain rate and initial temperatures of 77, 496, 696, 896, and 1096 K. Dotted curves represent the experimental data, long dash curves represent the continuum model calculation, and solid curves are the model calculation using the new crystal plasticity constitutive model, the proposed algorithm, and the Taylor averaging method.

and 0.001 s^{-1} for annealed and as-received OFHC copper is shown in Figs. 5 and 6, respectively.

6. Conclusions

A physically based rate- and temperature-dependent constitutive model is proposed in this work to model crystalline slip in fcc single crystals. The resistance to the motion of dislocations in single crystals is divided into a thermally activated part which is rate- and temperature-dependent, and an athermal part which is due to the stress field of all farfield dislocations and defects. Constitutive models are proposed for each part, based on the underlying physics of the process.

Then, a new algorithm is proposed to solve incrementally the finite-deformation problem of fcc single crystals. Two different computational methods are combined and used, depending on the deformation stages of the material. Three regimes of the material deformation history are defined. When the material is in the rapidly changing regime, where the elastic strains are comparable to the plastic ones, the explicit Euler method is applied. In the other regimes, where the elastic contribution is negligible, the *plastic-predictor*, *elastic-corrector* method is used, with their individual strategies for the transition regime and the steady-state regime, respectively. The proposed constitutive model and the computational algorithm are applied to simulate the response of polycrystalline OFHC copper over a broad range of strain rates, temperatures, and strains. A Taylor-type averaging scheme is used, and excellent correlation with experimental results is obtained using only a few

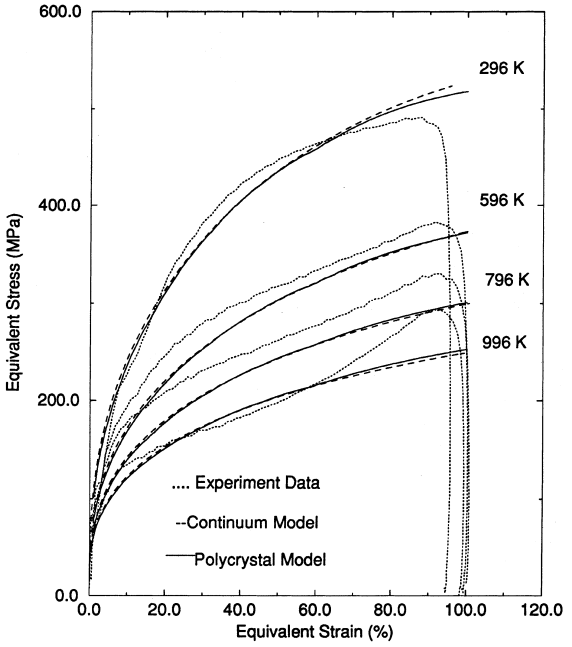

Fig. 3. Comparison between the experimental data, the continuum model calculation, and the crystal plasticity model calculation for polycrystalline annealed OFHC copper at 4000 s^{-1} strain rate and initial temperatures of 296, 596, 796, and 996 K. Dotted curves represent the experimental data, long dash curves represent the continuum model calculation, and solid curves are the model calculation using the new crystal plasticity constitutive model, the proposed algorithm, and the Taylor averaging method.

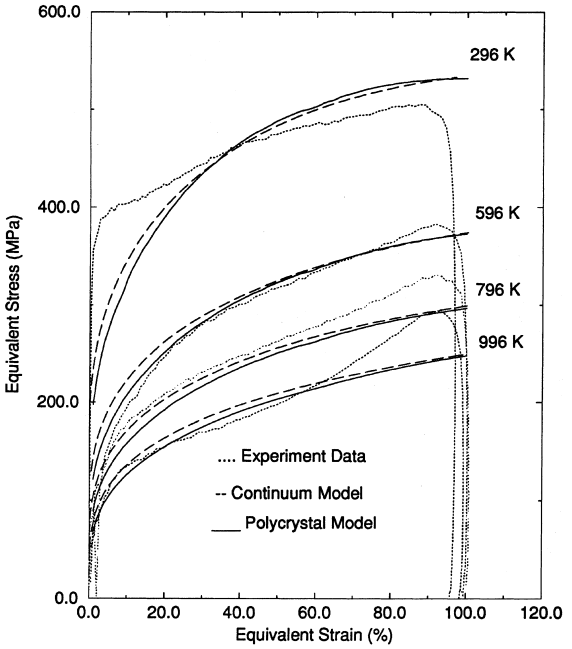

Fig. 4. Comparison between the experimental data, the continuum model calculation, and the crystal plasticity model calculation for polycrystalline as-received OFHC copper at 4000 s^{-1} strain rate and initial temperatures of 296, 596, 796, and 996 K. Dotted curves represent the experimental data, long dash curves represent the continuum model calculation, and solid curves are the model calculation using the new crystal plasticity constitutive model, the proposed algorithm, and the Taylor averaging method.

free constitutive parameters, which are fixed at the outset.

Acknowledgements

This research was supported by the Army Research Office under contract number ARO DAAL 03-92-G-0108 and ARO DAAL 03-96-I-0376 to the University of California, San Diego. The large-scale computations reported here were carried out on CRAY-C90 and CRAY-T90 at the San Diego Supercomputer Center.

Appendix A. Interdependency conditions

Define the following six second-order tensors:

$$\boldsymbol{N}^{(\mathrm{I})} = (\boldsymbol{e}_1 - \boldsymbol{e}_2) \otimes (\boldsymbol{e}_1 - \boldsymbol{e}_2), \tag{A.1a}$$

$$\boldsymbol{N}^{(\mathrm{II})} = (\boldsymbol{e}_1 + \boldsymbol{e}_3) \otimes (\boldsymbol{e}_1 + \boldsymbol{e}_3), \tag{A.1b}$$

$$\boldsymbol{N}^{(\mathrm{III})} = (\boldsymbol{e}_2 - \boldsymbol{e}_3) \otimes (\boldsymbol{e}_2 - \boldsymbol{e}_3), \tag{A.lc}$$

$$\boldsymbol{N}^{(\mathrm{IV})} = (\boldsymbol{e}_1 - \boldsymbol{e}_3) \otimes (\boldsymbol{e}_1 - \boldsymbol{e}_3), \tag{A.1d}$$

$$\boldsymbol{N}^{(\mathrm{V})} = (\boldsymbol{e}_2 + \boldsymbol{e}_3) \otimes (\boldsymbol{e}_2 + \boldsymbol{e}_3), \tag{A.le}$$

$$\boldsymbol{N}^{(\mathrm{VI})} = (\boldsymbol{e}_1 + \boldsymbol{e}_2) \otimes (\boldsymbol{e}_1 + \boldsymbol{e}_2), \tag{A.lf}$$

where $\boldsymbol{e}_i$, $i = 1, 2, 3$, define a fixed orthogonal unit triad in the three-dimensional Euclidean space.

From twelve slip systems of an fcc crystal, construct six classes of second-order tensors, say, Class I, Class II,..., Class VI, which are, respec-

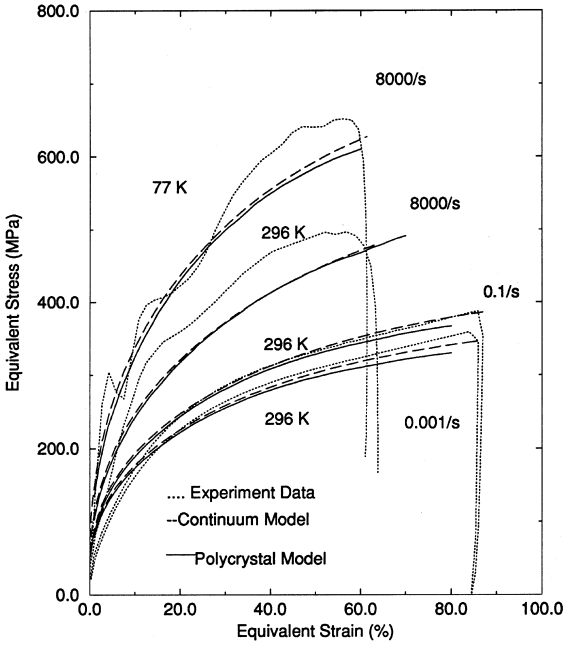

Fig. 5. Comparison between the experimental data, the continuum model calculation, and the crystal plasticity model calculation for polycrystalline annealed OFHC copper at strain rates of 8000, 0.1, and 0.001 s^{-1} and initial temperatures of 77 and 296 K. Dotted curves represent the experimental data, long dash curves represent the continuum model calculation, and solid curves are the model calculation using the new crystal plasticity constitutive model, the proposed algorithm, and the Taylor averaging method.

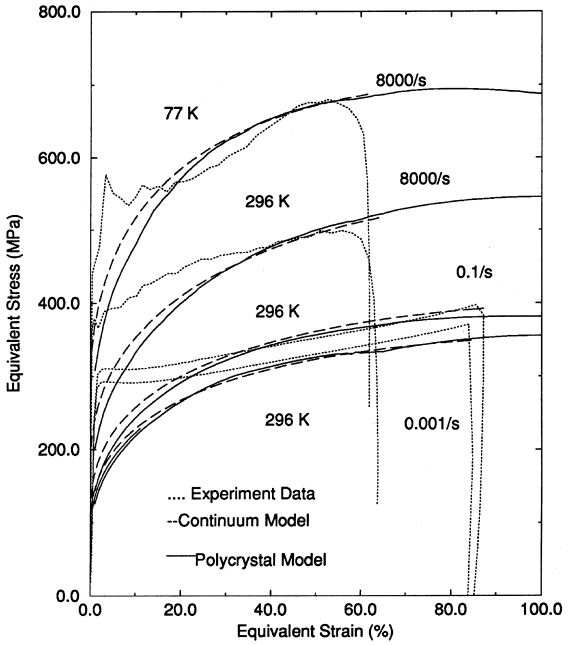

Fig. 6. Comparison between the experimental data, the continuum model calculation, and the crystal plasticity model calculation for polycrystalline as-received OFHC copper at strain rates of 8000, 0.1, and 0.001 s^{-1} and initial temperatures of 77 and 296 K. Dotted curves represent the experimental data, long dash curves represent the continuum model calculation, and solid curves are given by the model calculation using the new crystal plasticity constitutive model, the proposed algorithm, and the Taylor averaging method.

tively, orthogonal to the tensors $\boldsymbol{N}^{(\mathrm{I})}$, $\boldsymbol{N}^{(\mathrm{II})}$, …, $\boldsymbol{N}^{(\mathrm{VI})}$. The orthogonality here is defined by

$$\boldsymbol{a}_1 \otimes \boldsymbol{b}_1 : \boldsymbol{a}_2 \otimes \boldsymbol{b}_2 = (\boldsymbol{a}_1, \boldsymbol{a}_2)(\boldsymbol{b}_1, \boldsymbol{b}_2) = 0 \qquad \text{(A.2)}$$

with (,) denoting the usual inner-product of two three-dimensional vectors. Therefore, the members of each class can be easily identified by a simple inspection. For example, if $\boldsymbol{s}^{(\alpha)}$ or $\boldsymbol{n}^{(\alpha)}$ in $\boldsymbol{p}^{(\alpha)}$ is normal to the vector $\boldsymbol{e}_1 - \boldsymbol{e}_2$, then $\boldsymbol{p}^{(\alpha)}$ is orthogonal to $\boldsymbol{N}^{(I)}$. Using the numbering in Table 1, it is easy to verify that Class I contains

$$\boldsymbol{p}^{(11)}, \boldsymbol{p}^{(12)}, \boldsymbol{p}^{(13)}, \boldsymbol{p}^{(21)}, \boldsymbol{p}^{(31)}, \boldsymbol{p}^{(32)}, \boldsymbol{p}^{(33)}, \boldsymbol{p}^{(41)};$$

Class II contains

$$\boldsymbol{p}^{(13)}, \boldsymbol{p}^{(21)}, \boldsymbol{p}^{(22)}, \boldsymbol{p}^{(23)}, \boldsymbol{p}^{(31)}, \boldsymbol{p}^{(32)}, \boldsymbol{p}^{(33)}, \boldsymbol{p}^{(42)};$$

Class III contains

$$\boldsymbol{p}^{(11)}, \boldsymbol{p}^{(12)}, \boldsymbol{p}^{(13)}, \boldsymbol{p}^{(21)}, \boldsymbol{p}^{(22)}, \boldsymbol{p}^{(23)}, \boldsymbol{p}^{(32)}, \boldsymbol{p}^{(43)};$$

Class IV contains

$$\boldsymbol{p}^{(11)}, \boldsymbol{p}^{(12)}, \boldsymbol{p}^{(13)}, \boldsymbol{p}^{(22)}, \boldsymbol{p}^{(33)}, \boldsymbol{p}^{(41)}, \boldsymbol{p}^{(42)}, \boldsymbol{p}^{(43)};$$

Class V contains

$$\boldsymbol{p}^{(12)}, \boldsymbol{p}^{(23)}, \boldsymbol{p}^{(31)}, \boldsymbol{p}^{(32)}, \boldsymbol{p}^{(33)}, \boldsymbol{p}^{(41)}, \boldsymbol{p}^{(42)}, \boldsymbol{p}^{(43)};$$

Class VI is formed by

$$\boldsymbol{p}^{(11)}, \boldsymbol{p}^{(12)}, \boldsymbol{p}^{(13)}, \boldsymbol{p}^{(21)}, \boldsymbol{p}^{(22)}, \boldsymbol{p}^{(23)}, \boldsymbol{p}^{(32)}, \boldsymbol{p}^{(43)}.$$

Note that the classes have some common elements.

Assume the 12 slip systems linearly span a space $\mathscr{E}^5$, which is of at most five dimensions, as discussed in Section 2.2. Then, each of the above-defined classes spans a four dimensional subspace of $\mathscr{E}^5$, in view of the corresponding orthogonality. Denote these subspaces by $\mathscr{V}^{\mathrm{I}}$, $\mathscr{V}^{\mathrm{II}}, \ldots, \mathscr{V}^{\mathrm{VI}}$, corresponding to Class I, Class II,…, Class VI, respectively. Hence, the intersection of $\mathscr{V}^{\mathrm{I}}$, $\mathscr{V}^{\mathrm{II}}$,

and $\mathscr{V}^{\mathrm{III}}$ gives a two-dimensional subspace, which, in particular, contains $\boldsymbol{p}^{(13)}$, $\boldsymbol{p}^{(21)}$, and $\boldsymbol{p}^{(32)}$. Thus those slip systems are linearly dependent, and a linear interdependency condition (2.10c) exists between them.

In a similar manner, $\mathscr{V}^{\mathrm{I}} \bigcap \mathscr{V}^{\mathrm{IV}} \bigcap \mathscr{V}^{\mathrm{V}}$ gives the linear interdependency relation (2.10b) between $\boldsymbol{p}^{(12)}$, $\boldsymbol{p}^{(33)}$, and $\boldsymbol{p}^{(41)}$, and $\mathscr{V}^{\mathrm{III}} \bigcap \mathscr{V}^{\mathrm{IV}} \bigcap \mathscr{V}^{\mathrm{VI}}$ gives the linear interdependency relation (2.10a) between $\boldsymbol{p}^{(11)}$, $\boldsymbol{p}^{(22)}$, and $\boldsymbol{p}^{(43)}$.

References

Anand, L., Kalidindi, S.R., 1994. The process of shear band formation in plane strain compression of fcc metals: effects of crystallographic texture. Mech. Mater. 17, 223–243.

Chen, S.R., Gray III, G.T., 1996. Constitutive behavior of tantalum and tantalum-tungsten alloys. Metall. Mater. Trans. A 27A, 2994–3006.

Havner, K.S., 1992. Finite Plastic Deformation of Crystalline Solids. Cambridge, New York.

Hill, R., 1966. Generalized constitutive relations for incremental deformation of metal crystals by multislip. J. Mech. Phys. Solids 14, 95–102.

Hill, R., Havner, K.S., 1982. Perspectives in the mechanics of elasto-plastic crystals. J. Mech. Phys. Solids 30, 5–22.

Hill, R., Rice, J.R., 1972. Constitutive analysis of elastic–plastic crystals at arbitrary strain. J. Mech. Phys. Solids 20, 401–413.

Hutchinson, J.W., 1976. Bounds and self-consistent estimates for creep of polycrystalline materials. Proc. Roy. Soc. London A 348, 101–127.

Kapoor, R., Nemat-Nasser, S., 1998. Determination of temperature rise during high strain rate deformation. Mech. Mater. 27, 1–12.

Kocks, U.F., Argon, A.S., Ashby, M.F., 1975. Thermodynamics and kinematics of slip. In: Progress in Materials Science, vol. 19. Pergamon Press, Oxford.

Nemat-Nasser, S., 1996. Plasticity: Inelastic flow of heterogeneous solids at finite strains and rotations. In: Proceedings of the ICTAM Kyoto, Elsevier, Amsterdam, pp. 25–31.

Nemat-Nasser, S., 1998. Plasticity: A Treatise on Finit Deformation of Heterogeneous Inelastic Solids. In preparation.

Nemat-Nasser, S., Isaacs, J.B., 1997. Direct measurement of isothermal flow stress of metals at elevated temperatures and high strain rates with application to Ta and Ta–W alloys. Acta Metall. 45, 907–919.

Nemat-Nasser, S., Li, Y., 1998. Flow stress of f.c.c. polycrystals with application of OFHC Cu. Acta Mater. 46 (2), 565–577.

Nemat-Nasser, S., Obata, M., 1986. Rate dependent, finite elastoplastic deformation of polycrystals. Proc. Roy. Soc. London A 407, 343–375.

Nemat-Nasser, S., Okinaka, T., 1996. A new computational approach to crystal plasticity: fcc single crystal. Mech. Mater. 24, 43–57.

Nemat-Nasser, S., Okinaka, T., Ni, L., 1998. A physically-based constitutive model for bcc crystals with application to polycrystalline tantalum. J. Mech. Phys. Solids 46, 1009–1038.

Ono, K., 1968. Temperature dependence of dislocation barrier hardening. J. Appl. Phys. 39, 1803–1806.

Pan, J., Rice, J.R., 1983. Rate sensitivity of plastic flow and implications for yield-surface vertices. Int. J. Solids Struct. 19, 973–987.

Peirce, D., Asaro, R.J., Needleman, A., 1983. Material rate dependence and localized deformation in crystalline solids. Acta. Metall. 31, 1951–1976.

Rashid, M.M., Gray III, G.T., Nemat-Nasser, S., 1992. Heterogeneous deformations in copper single crystals at high and low strain rates. Phil. Mag. 65, 707–735.

Rice, J.R., 1971. Inelastic constitutive relations for solids: an internal variable theory and its application to metal plasticity. J. Mech. Phys. Solids. 19, 433–455.

Stroh, A.N., 1953. The mean shear stress in an array of dislocations and latent hardening. Proc. Phys. Soc. B 66, 2–6.

Zarka, J., 1968. Sur la viscoplasticité des métaux. Ph.D. Thesis, Paris.

Zikry, M.A., Nemat-Nasser, S., 1990. High strain-rate localization and failure of crystalline materials. Mech. Mater. 10, 215–237.